A honeycomb-like predictive controller with a reduced computational burden for three-level NPC converters

José Silva, Jaime Rohten, Felipe Villarroel, Esteban Pulido and Marco Rivera

***Abstract*—This paper presents a predictive control strategy to control a photovoltaic plant based on bifacial photovoltaic (BPV) panels connected to the electrical grid through a three-phase neutral point clamped (NPC) power converter. Electricity generation plants based on non-conventional renewable energies are affected by the availability of the natural resource and grid changes. To achieve optimal use of natural resources and equipment, BPV cells must operate at the maximum power point and the currents injected into a grid must be in phase with the voltages. Due to the high number of states, one important drawback of conventional predictive control in the NPC converter is its computational burden. The proposed controller avoids the use of a cost function and can achieve the same control objectives with only 20% of the computational cost of the conventional strategy. To achieve this reduction the proposed strategy exploits the operating area of the converter, separating the possible voltages in hexagons, which results in a shape like a honeycomb. Simulation and experimental results show the feasibility of the proposed method in different operating conditions.**

***Index Terms*—Solar power generation, AC-DC power converters, multilevel converters, predictive control.**

I. INTRODUCTION

IN recent years, the current price of the photovoltaic (PV) cells has dropped considerably [1], and their efficiency has increased; these last two factors favor the use of this technology on a large scale [2] since the cost of generating electricity has become competitive compared to traditional generation systems [3]. On the other hand, the advance of PV technology has led to the development of bifacial photovoltaic cells (BPV), which have the capacity to capture solar energy on both sides of the cell plate [4] and therefore are capable of harvest more solar energy to inject into the electric mains.

Multilevel power converters are capable of generating better quality AC voltages and currents than converters with fewer levels, and make them suitable for high-voltage and high-power applications [5], but are more complex to control due to the greater number of switches they have. Among them, neutral point clamped (NPC) converters [6], [7], as shown in Fig. 1 (a),

are widely employed in PV generation systems [8].

The finite-set model predictive controller (FS-MPC) [9], also named finite control set model predictive control (FCS-MPC), is emerging as an attractive option for the control of NPC power converters [10], because it does not have the complexity of multilevel modulation techniques [11]. Furthermore, it offers a fast dynamic response, simple inclusion of nonlinearities and constraints, and multivariable control capabilities [9]. However, a big drawback of its application in NPC power converters is its computational burden, given that NPC three-level converters have 27 voltage vectors [12]. Then, it is imperative to reduce the computation requirements. This problem increases as the level increases because the NPC has more states, for example the 5 level NPC has 125 states (61 voltages) and the 7 level NPC has 347 states (127 voltages) and therefore the evaluation of each state will make it impossible to apply the FS-MPC because the digital board will not be able to process each prediction within the sampling time.

In [13] a new concept No-Iteration-MPC (NI-MPC) is proposed to simplify the implementation of a FS-MPC for an AFE converter (8 states), which does not require a cost function, present a 43% reduction in the computational cost, and has the same behavior in the output electrical variables with respect to the FS-MPC conventional method. However, this work does not present the formulation of this concept for other more complex converter topologies, especially those with a significant number of states, where the computational effort when using a cost function is much higher.

To address these shortcomings, this work formulates, tests, and evaluates the feasibility of the NI-MPC concept for an NPC type converter (27 states), including the additional complexity that this topology introduces in the control of capacitor voltage unbalance. The proposed strategy can operate the BPV cells at their maximum power point (MPP). This is achieved adjusting the DC voltage level to the maximum power point voltage v_{mpp}, as estimated by a maximum power point tracking (MPPT) algorithm [14]–[17]. In addition, the strategy is able to balance the voltage on the DC link capacitors [7], [12], [18], which is a key issue on the voltage and current distortions [12] as a result of voltages deviation from equality [19]. Consequently, it allows the NPC converter to achieve lower distortion waveforms in the AC network, injecting the energy generated
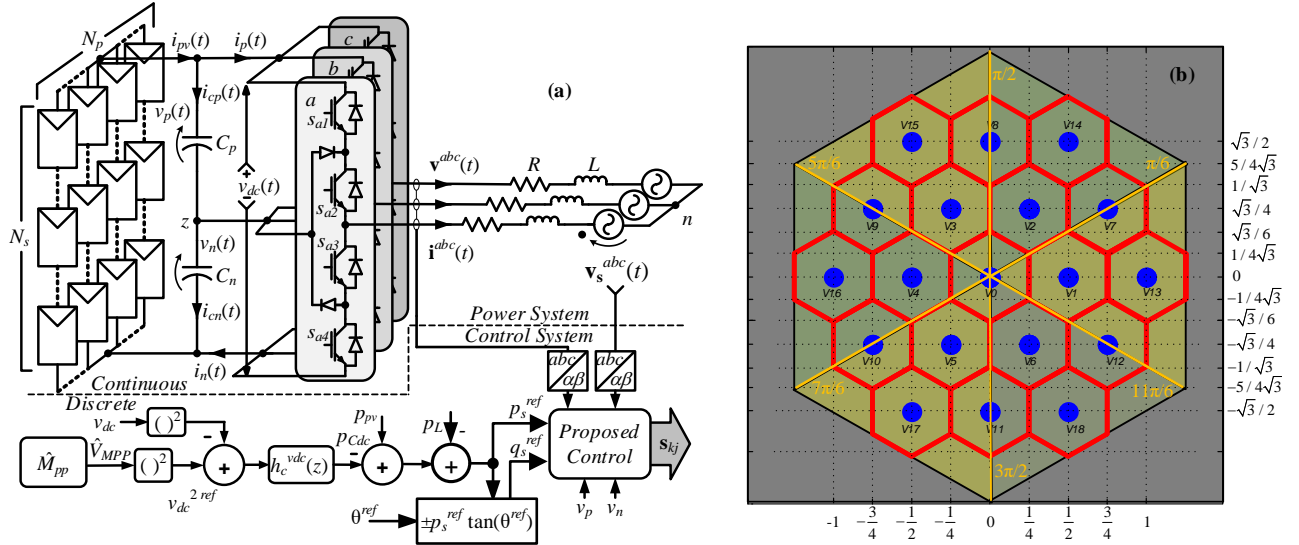
Fig. 1. Power converter system. (a) converter topology and controller block diagram, (b) valid converter switching states.

by the BPV cells with the required frequency level and power factor.

One of the main contributions of this work is the proposal of a new technique that significantly reduces the computational cost to control an NPC converter using BFV cells, allowing to implement the entire control algorithm in common commercial devices. Pointing out toward this goal, a state selection mechanism based on the partitioning of the valid voltage vector space of the NPC converter, Fig. 1 (a), in a network of hexagons as shown in Fig. 1 (b) is proposed. Thus, a honeycomb-like figure is formed, similar to bee panels. Thanks to this geometric shape a fast, efficient, and low computational cost predictive controller is achieved.

The rest of the article is structured as follows. Section II establishes the mathematical model and general control aspects of the generation system. Section III discusses the proposed predictive control strategy, including a brief summary of the conventional one. Section IV verifies the feasibility of the proposal using simulation and experimental tests in a prototype power converter system, subjecting the system to different operating conditions.

II. PV SYSTEM MODEL AND CONTROL

A. Continuous-time Representation of the Power Converter

The NPC power converter injects a five-level line-to-line voltage to the grid side, reducing the THD on the electric variables. From Fig. 1 the converter ac side can be modeled as:

$$\mathbf{v}^{abc} = L\frac{d}{dt}\mathbf{i}^{abc} + R\mathbf{i}^{abc} + \mathbf{v}_s^{abc}, \qquad (1)$$

where the injected voltage is given by:

$$\mathbf{v}^{abc} = \mathbf{s}_1^{abc}v_p + \left(\mathbf{s}_2^{abc} - \mathbf{1}\right)v_n + \mathbf{1}v_{zn}, \qquad (2)$$

with $\mathbf{1} = [1\ 1\ 1]^T$. The dc side model is obtained by the current summation in the upper and bottom point:

$$i_{pv} = i_p + C_p\frac{dv_p}{dt} = i_n + C_n\frac{dv_n}{dt}, \qquad (3)$$

where i_p and i_n are calculated as:

$$i_p = \left\langle \mathbf{i}^{abc}, \mathbf{s}_1^{abc} \right\rangle, \quad i_n = \left\langle \mathbf{i}^{abc}, \mathbf{s}_2^{abc} \right\rangle - \left\langle \mathbf{i}^{abc}, \mathbf{1} \right\rangle, \qquad (4)$$

where $\langle \cdot, \cdot \rangle$ represents the dot product. The equations can be rewritten in the $\alpha\beta0$ frame using the corresponding transformation [20].

B. BPV array model

The photovoltaic array is modeled based on the single cell shown in Fig. 2. To get higher power, the cell array is composed by N_p strings in parallel, where each string has N_s cells in series. The current produced by the BPV array is:

$$i_{pv} = I_{sco}\frac{S}{S_o}N_p - I_oN_p\left(e^{\left(\frac{v_d^T/N_s}{nkT}q\right)} - 1\right) - \frac{v_d^T/N_s}{R_{sh}N_p}, \qquad (5)$$

where I_{SCO}, S_O, I_O, n, k, q, R_s, R_{sh} are the cells parameters, v_d is the diode voltage, i_{pv} is the PV array supply current, S represents the solar irradiation, and T the cell temperature. Assuming that the irradiation and temperature conditions are equal for all cells, the power delivered by the array is:

$$p_{pv} = i_{pv}v_{dc} = f\left(T, S, v_{dc}\right). \qquad (6)$$

where $v_{dc} = v_p + v_n$.

C. MPPT Algorithm

To operate at MPP the voltage v_{dc} at the terminals of the solar array is adjusted. This is achieved by a power controller that changes the amount of power injected to the grid. If the voltage needs to be decreased, the amount of power injected to the grid is increased and vice versa. Thus, the v_{dc} must track the MPP voltage (v_{MPP}), which needs to be imposed by a MPPT algorithm [14], [15]. To this end, this paper uses a direct method
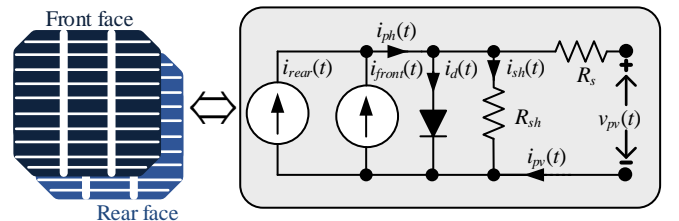

Fig. 2. Bifacial photovoltaic cell representation.

that relies on measuring cells to obtain the MPP voltage. The temperature and the solar irradiance are estimated and then used together with the cell's model to calculate the MPP voltage. The procedure is detailed in [16], [17].

This work uses a direct method based on the measurement cells to reach the MPP. Basically, it is necessary to measure the open circuit voltage (v_{oc}) and a short circuit current (i_{sc}) from two measuring cells, and based on the cell's mathematical model, the current i_{ph} and the junction temperature are estimated to calculate the maximum power voltage. The procedure is detailed in [16], [17], but it is worthy to mention that the estimations are made by two observers regulated by a PI controllers that allows to twin the cell's behavior into a computing model.

D. DC Voltage and Power Factor Control

The renewable energy injection demands an active power control at the grid side. In addition, the system can inject a phase-shifted current which may be used to compensate reactive power or even for voltage amplitude regulation. The power converter control obeys the power balance among all the units in the system of Fig. 1. The power provided by the solar array p_{pv} provides the power to supply the capacitor state of charge p_{Cdc}, the RL losses in the topology p_L, and the final power injected to the grid p_s, in other words:

$$p_{pv} = p_{Cdc} + p_L + p_s. \tag{7}$$

The power due to the capacitor state of charge is managed by the dc voltage control. This can be achieved by a linear proportional-integral, $h_c^{vdc}(z)$, controller, which allows zero steady state error and is given by:

$$p_{Cdc}(k) = p_{Cdc}(k-1) + k_c^{vdc}\left(1 + \frac{T_s}{2T_i^{vdc}}\right)e^{vdc}(k) + \cdots$$
$$k_c^{vdc}\left(-1 + \frac{T_s}{2T_i^{vdc}}\right)e^{vdc}(k-1) \tag{8}$$

where k_c^{vdc} and T_i^{vdc} are the PI controller parameters, T_s is the sampling time and $e^{vdc}(k) = v_{dc}^{ref\,2}(k) - v_{dc}^{\,2}(k)$. Thus, the reference active power to be injected is given by:

$$p_s^{\,ref}(k) = p_{pv}(k) - p_{Cdc}(k) - p_L(k). \tag{9}$$

where p_{pv} is the solar power, p_L is the RL filter power.

On the other hand, the reactive power depends on the phase-shift between the current and voltage at the grid side. The relationship of the phase-shift with the reactive power reference can be defined as:

$$q_s^{\,ref}(k) = p_s^{\,ref}(k)\tan\left(\theta^{ref}(k)\right). \tag{10}$$

where θ^{ref} represents the shift angle between the voltage $\mathbf{v_s}^{abc}$ and the current $\mathbf{i}^{abc}$.

III. PROPOSED PREDICTIVE CONTROL STRATEGY

The power references given by the power injection control also define the grid currents, because the grid voltage is considered as a disturbance. Therefore, the power control can be achieved by imposing a current from the grid lines using an inner control loop. The most employed options are linear, nonlinear, resonant, and predictive control. Predictive control is an attractive alternative among them, due to its simple concept
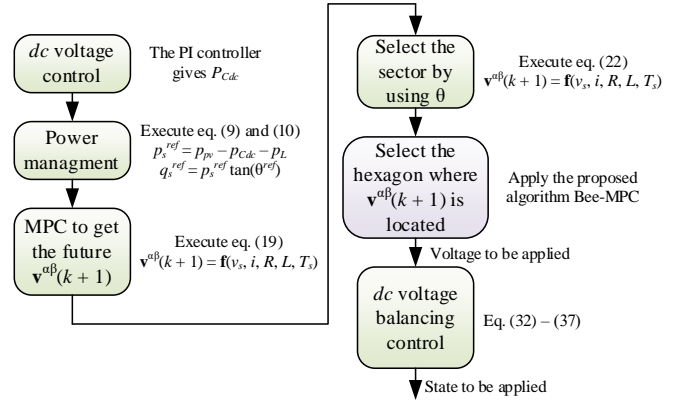
Fig. 3. Proposed algorithm overview.

and high dynamic performance. In particular, finite set model predictive control (FS-MPC), which employs the discrete number of switching states to choose the best one in order to follow the reference [21], is the most favored option [22]. However, one of its biggest drawbacks is its computational requirements as a prediction must be computed for every single valid state, which is an issue particularly on multilevel topologies such as NPC converters. To address the problem, a new algorithm will be proposed that reduces the computational burden by avoiding the iterative procedure of FS-MPC.

A. Finite Set Model Predictive Control

FS-MPC uses the power converter model to predict the current in the near future by trying all possible states. To accomplish the prediction the model needs to be discretized, where a forward Euler approximation is commonly used [21], [23]. The model gives the relationship between the present and futures variables as

$$\mathbf{i}^{\alpha\beta}(k+1) = \left(1 - (T_s R / L)\right)\mathbf{i}^{\alpha\beta}(k) + \cdots$$
$$(T_s / L)\begin{pmatrix}\mathbf{v_s}^{\alpha\beta}(k) - \mathbf{s_1}^{abc}(k)v_p(k) - \cdots \\ \left(\mathbf{s_2}^{abc}(k) - \mathbf{1}\right)v_n(k) - \mathbf{1}v_{Nn}(k)\end{pmatrix}, \tag{11}$$

where an additional prediction at time $k + 2$ is used to mitigate the effects of the digital board processing time [24], requiring the left side variables at $k + 1$. The grid voltage at instant $k + 1$, $\mathbf{v_s}^{\alpha\beta}(k + 1)$, which can be obtained as:

$$\hat{v}_s^{\,\alpha\beta}(k+1) = e^{2\pi f T_s}\vec{v}_s^{\,\alpha\beta}(k). \tag{12}$$

Furthermore, voltages v_p, v_n and v_{Nn} can be directly derived discretizing (3) and (2), respectively.

Then, the power prediction can be computed from the currents as:

$$\hat{p}(k+2) = \hat{v}_s^{\,\alpha}(k+2)\hat{i}^{\alpha}(k+2) + \hat{v}_s^{\,\beta}(k+2)\hat{i}^{\beta}(k+2), \tag{13}$$

$$\hat{q}(k+2) = \hat{v}_s^{\,\beta}(k+2)\hat{i}^{\alpha}(k+2) - \hat{v}_s^{\,\alpha}(k+2)\hat{i}^{\beta}(k+2), \tag{14}$$

where the current is obtained as an additional prediction using (11), and the voltage as the extrapolation in (12).

Lastly, a cost function is defined to minimize the tracking power error by choosing among all possible voltages $\mathbf{v}^{\alpha\beta}$, as:

$$g_1 = \left|p^{ref} - \hat{p}(k+2)\right| + \left|q^{ref} - \hat{q}(k+2)\right|. \tag{15}$$

An important issue of the NPC topology of Fig. 1 is that the capacitor voltages can diverge or be different, and therefore a
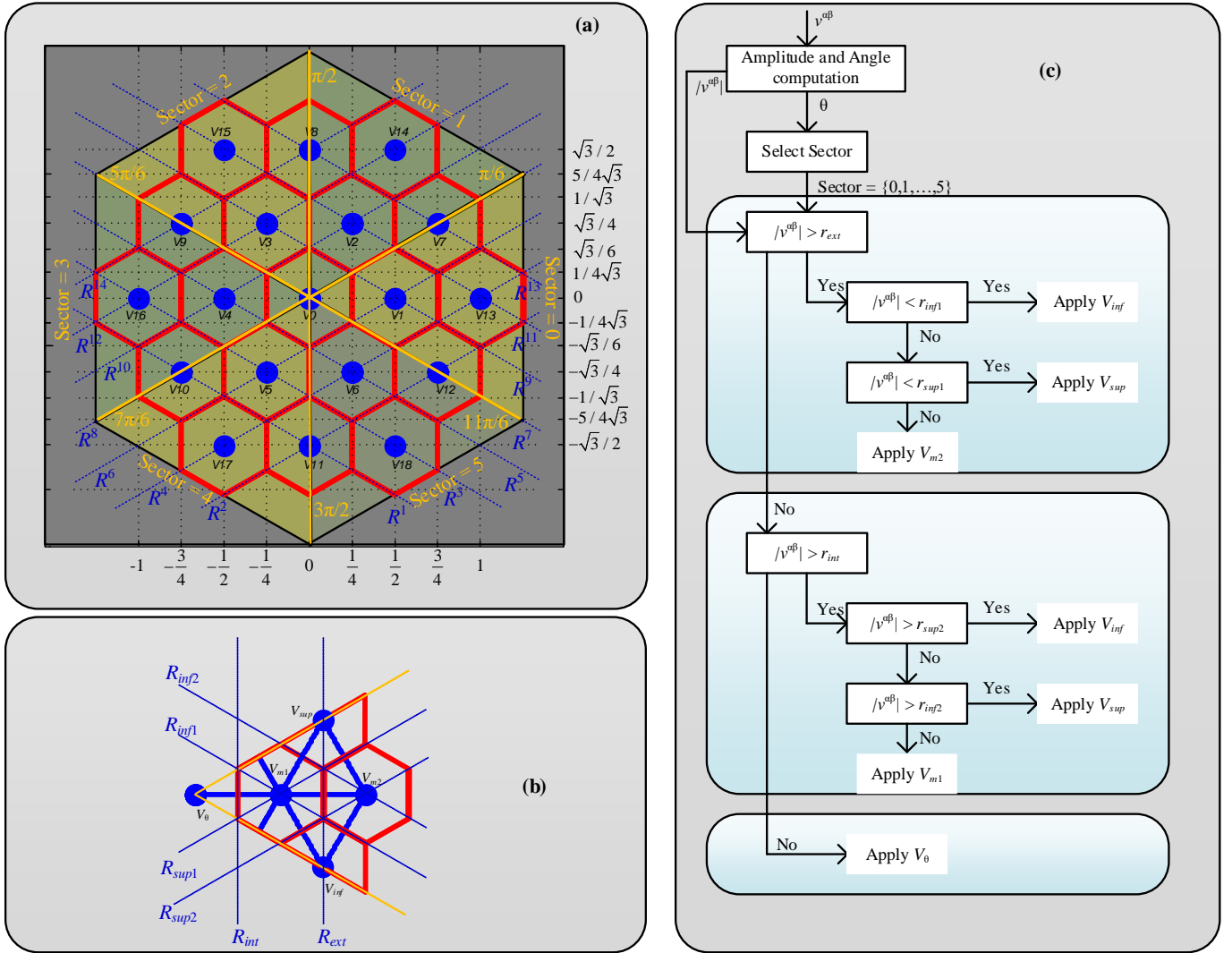
Fig. 4. NPC voltages, (a) honeycomb array, (b) one sector highlight, (c) algorithm.

balancing method is required. The controller should choose among the redundant states to minimize the voltage difference between v_p and v_n, which follows from the discretization of (3) as:

$$\Delta \hat{v}_{dc}\left(k+2\right)=\Delta \hat{v}_{dc}\left(k+1\right)+\frac{T_s}{C_p}\left(\hat{i}_n\left(k+1\right)-\hat{i}_p\left(k+1\right)\right). \quad (16)$$

Then, the associated second cost function is:

$$g_2 = \left|\Delta \hat{v}_{dc}\left(k+2\right)\right|. \quad (17)$$

To reduce the required calculations in the NPC converter, algorithm is divided in two steps, first selecting among the 18 active voltages, then considering the redundant states. This way, instead of 27 evaluations, only 19 plus two or three evaluations are performed if the zero voltage is required. Details of this traditional FS-MPC can be found in the following references [25]–[28].

B. Proposed Honeycomb based algorithm

To mitigate the high computation requirements of FS-MPC, a new algorithm Bee-MPC is proposed that has the same capabilities but avoids the costly iterations reducing the computational effort. The algorithm uses the optimal voltage given by a prediction according to the currents desired at time $k+2$ and chooses the nearest valid state, and also allows to regulate the *dc* voltage unbalance. A summary of the proposed control is depicted in Fig. 3, detailing the steps the algorithms perform.

The Bee-MPC formulation starts from (1) with the aim to determine the voltage required to track the current reference as:

$$\mathbf{v}^{abc}\left(k\right)=\frac{L}{T_s}\left(\mathbf{i}^{abc}\left(k+1\right)-\mathbf{i}^{abc}\left(k\right)\right)+R\mathbf{i}^{abc}\left(k\right)+\mathbf{v}_s^{abc}\left(k\right), \quad (18)$$

and considering the computational delay:

$$\mathbf{v}^{\alpha\beta}\left(k+1\right)=\frac{L}{T_s}\left(\mathbf{i}^{\alpha\beta}\left(k+2\right)-\mathbf{i}^{\alpha\beta}\left(k+1\right)\right)+\cdots \\ R\mathbf{i}^{\alpha\beta}\left(k+1\right)+\mathbf{v}_s^{\alpha\beta}\left(k+1\right) \quad , \quad (19)$$

where $\mathbf{i}^{\alpha\beta}(k + 1)$ is obtained as (11), $\mathbf{v}_s^{\alpha\beta}(k + 1)$ as (12), and $\mathbf{i}^{\alpha\beta}(k + 2)$ is set as the reference. The current reference can be derived from the active and reactive power reference as:

$$\mathbf{i}^{\alpha\beta,\,ref}\left(k\right)=\frac{1}{\left\|\mathbf{v_s}^{\alpha\beta}\left(k\right)\right\|_2^2}\begin{bmatrix}\mathrm{Re}\left\{\vec{s}_{pq}^{\,ref*}\left(k\right)\cdot\vec{v}_s^{\,\alpha\beta}\left(k\right)\right\}\\ \mathrm{Im}\left\{\vec{s}_{pq}^{\,ref*}\left(k\right)\cdot\vec{v}_s^{\,\alpha\beta}\left(k\right)\right\}\end{bmatrix}, \quad (20)$$

where $\left\|\cdot\right\|_2$ represents the 2-norm and the apparent power is defined as:

$$\vec{s}_{pq}^{\ ref}(k) = p^{ref}(k) + jq^{ref}(k), \qquad (21)$$

and $\vec{s}_{pq}^{\ ref\,*}$ is conjugate of the apparent power.

Once the voltage to be applied in the next step $\mathbf{v}^{\alpha\beta}(k+1)$ is computed, the nearest state is applied. Thus, the αβ states plane is divided by the possible voltages. The separation around every valid voltage emerges as the bee honeycomb hexagon as shown in Fig. 4 (a).

First step is to position in which sector of Fig. 4 (a) the voltage $\mathbf{v}^{\alpha\beta}$ is placed and its respective angle θ, where:

$$\theta = \arg\{\mathbf{v}^{\alpha\beta}\} = \mathrm{sgn}(v^\beta)\arccos\left(\frac{v^\alpha}{\left|\mathbf{v}^{\alpha\beta}\right|}\right), \qquad (22)$$

employing the four-quadrant argument function arg{}. The sectors are divided into 6 parts and separated as:

$$\begin{cases} \text{Sector} = 0, & \text{if} & -\pi/6 \le \theta < \pi/6 \\ \text{Sector} = 1, & \text{if} & \pi/6 \le \theta < \pi/2 \\ \text{Sector} = 2, & \text{if} & \pi/2 \le \theta < 5\pi/6 \\ \text{Sector} = 3, & \text{if} & 5\pi/6 \le \theta < 7\pi/6 \\ \text{Sector} = 4, & \text{if} & 7\pi/6 \le \theta < 3\pi/2 \\ \text{Sector} = 5, & \text{if} & 3\pi/2 \le \theta < 11\pi/6 \end{cases} \qquad (23)$$

Once the sector is selected, then a valid voltage needs to be chosen.

Note that all sectors have the same structure, where 6 new lines have been declared: R_{int}, R_{ext}, R_{sup1}, R_{sup2}, R_{inf1}, R_{inf2}, these will separate the different valid voltages, as seen in Fig. 4 (b) in order to determine the set of valid voltages V_{sup}, V_{inf}, V_θ, V_{m1}, V_{m2} to be applied. To decide which voltage to apply, the algorithm of Fig. 4 (c) is employed which may be extended for any sector, where the valid voltage is selected directly without the need of iterations. In fact, the lines can be defined for every sector as specified in Table I.

The 19 lines that divide the valid voltages honeycomb of Fig. 4 (a) are named as R^i with $i = \{0,1,2,\ldots,19\}$ where $i =$

TABLE I
BOUNDARY LINES DEFINITIONS PER SECTOR

Sector	R_{int}	R_{ext}	R_{inf1}	R_{inf2}	R_{sup1}	R_{sup2}
0	R^{14}	R^{16}	R^9	R^{11}	R^4	R^2
1	R^9	R^{13}	R^8	R^{10}	R^{15}	R^{17}
2	R^8	R^{12}	R^{14}	R^{16}	R^9	R^{11}
3	R^{14}	R^{18}	R^5	R^3	R^8	R^{10}
4	R^1	R^5	R^4	R^2	R^{14}	R^{16}
5	R^4	R^0	R^{15}	R^{17}	R^7	R^5

$\{0,1,\ldots,12\}$ are the positive slope lines, $i = \{1,2,\ldots,13\}$ are the negative slope lines, and $i = \{14,15,\ldots,19\}$ are the vertical lines. Each line is defined by the first-order function:

$$R^i : v^\beta = m^i v^\alpha + b_i, \qquad (24)$$

where the lines are separated as follow:

$$R^{2l+1} : v^\beta = -\frac{1}{\sqrt{3}} v^\alpha + \frac{l-3}{2\sqrt{3}}, l = \{0,1,\ldots,6\}, \qquad (25)$$

$$R^{2l} : v^\beta = \frac{1}{\sqrt{3}} v^\alpha + \frac{l-3}{2\sqrt{3}}, l = \{0,1,\ldots,6\}, \qquad (26)$$

$$R^{14} : v^\alpha = -\frac{1}{4}, R^{15} : v^\alpha = \frac{1}{4}, R^{16} : v^\alpha = -\frac{1}{2}, \qquad (27)$$
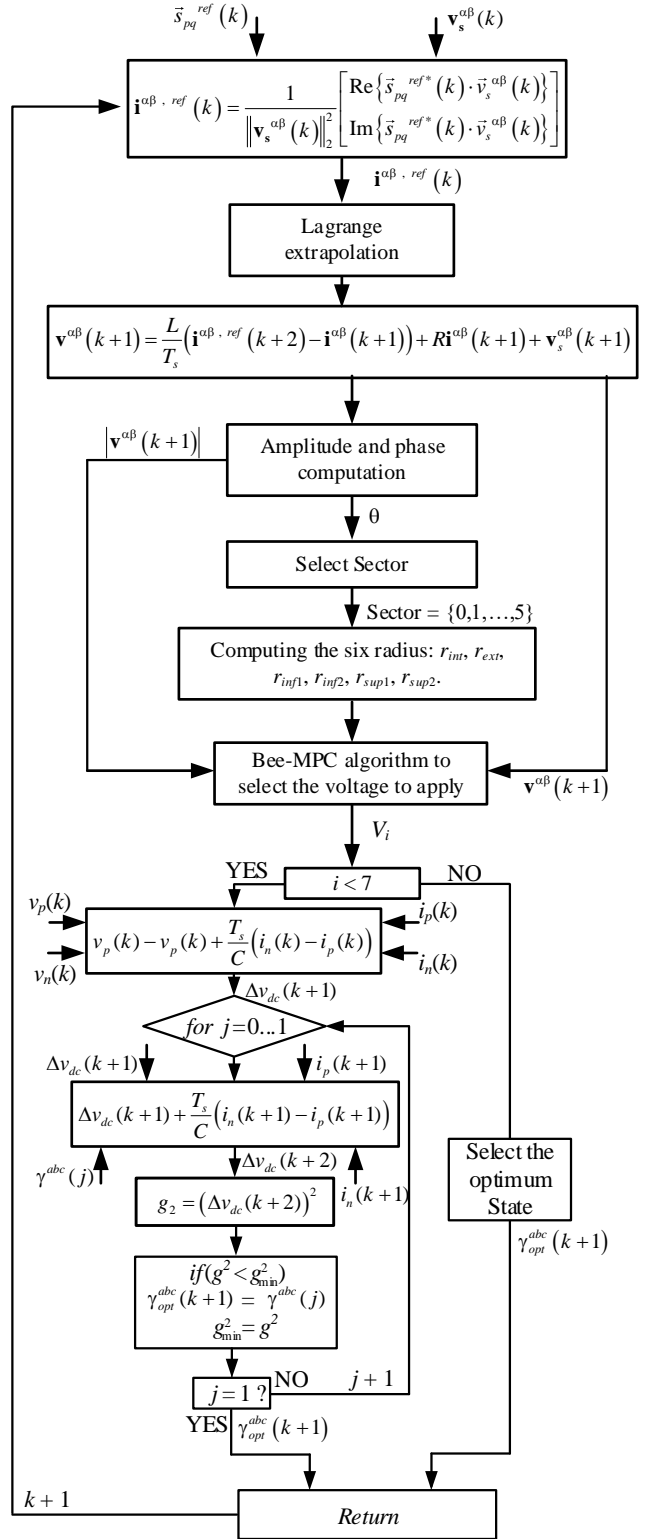

Fig. 5. Flowchart of the proposed Honeycomb based FS-MPC control algorithm for the NPC converter.

$$R^{17} : v^\alpha = \frac{1}{2}, R^{18} : v^\alpha = -\frac{3}{4}, R^{19} : v^\alpha = \frac{3}{4}. \qquad (28)$$

Equation (24) can be transformed into polar coordinates as:

$$v^\alpha = r_i \cos(\theta), v^\beta = r_i \sin(\theta) \quad i = \{0,1,\ldots,13\}, \qquad (29)$$

where:

$$r_{2l+1} = \frac{1}{4} \frac{l-3}{\sin(\theta + \pi/6)}, \qquad l = \{0,1,...,6\}, \qquad (30)$$

$$r_{2l} = \frac{1}{4} \frac{l-3}{\sin(\theta - \pi/6)}, \qquad l = \{0,1,...,6\}. \qquad (31)$$

Then, the voltage selection can be implemented by successive *if* conditionals, with lower computational requirements.

To balance the capacitor voltages the short and zero voltages are employed, *i.e.*, from V_0 up to V_6, Fig. 4 (a). Then, (3) is employed in order to predict the voltage behavior:

$$v_m(k+1) \approx \hat{v}_m(k+1) = v_m(k) + \frac{T_s}{C_m}\left(i_{dc}(k) - i_m(k)\right), \quad (32)$$

where $m = \{p, n\}$. The voltage difference between v_p and v_n, assuming that $C_p = C_n = C$, becomes

$$\Delta\hat{v}_{dc}(k+1) = v_p(k) - v_n(k) + \frac{T_s}{C}\left(i_n(k) - i_p(k)\right). \qquad (33)$$

As the calculated states are to be applied in the time $k + 1$, the voltage difference in (33) needs to be one step forwarded

$$\Delta\hat{v}_{dc}(k+2) = \Delta\hat{v}_{dc}(k+1) + \frac{T_s}{C}\left(\hat{i}_n(k+1) - \hat{i}_p(k+1)\right). \quad (34)$$

On the other hand, the prediction of the currents i_n and i_p are obtained from (4) as:

$$\hat{i}_p(k+1) = \left\langle \hat{\mathbf{i}}^{abc}(k+1), \mathbf{s}_1^{abc}(k+1) \right\rangle, \qquad (35)$$

TABLE II
NUMBER OF OPERATIONS FOR EVERY ALGORITHM

Algorithm	Operation	Number of operations	Time to evaluate
FS-MPC Algorithm	**Main loop (19 cycles)**		
	Sums	10	26.7 ns×10×19
	Subtractions	11	33.4 ns×11×19
	Multiplications	20	60.0 ns×20×19
	Magnitude	2	280.0 ns×2×19
	For, if, and other instructions	10	26.7 ns×10×19
	***dc* voltage balancing loop (2 cycles)**		
	Sums	10	26.7 ns×10×2
	Subtractions	11	33.4 ns×11×2
	Multiplications	20	60.0 ns×20×2
	for, *if, and other simpler instructions*	8	26.7 ns×8×2
	Total Time		**49.34 μs**
Bee-MPC Algorithm	**Bee-MPC, direct calculation**		
	Sums	15	26.7 ns×7×1
	Subtractions	18	33.4 ns×10×1
	Multiplications	41	60.0 ns×17×1
	Divisions	3	220 ns×3×1
	for, *if, and other simpler instructions*	22	26.7 ns×12×1
	arccos(·)	1	410 ns×1×1
	sin(·)	2	410 ns×2×1
	Magnitude	1	280 ns×1×1
	***dc* voltage balancing loop (2 cycles)**		
	Sums	4	26.7 ns×4×2
	Subtractions	4	33.4 ns×4×2
	Multiplications	12	60.0 ns×12×2
	for, *if, and other simpler instructions*	5	280 ns×5×2
	Total Time		**8.75 μs**

TABLE III
NUMBER OF OPERATIONS FOR EVERY ALGORITHM

Operation	FS-MPC	Bee-MPC	Percentage
Sums	210	23	11%
Subtractions	231	26	11%
Multiplications	420	65	15%
Magnitude	38	1	3%
For, if, and other instructions	206	32	16%
arccos(·)	0	1	-
sin(·)	0	2	-
	Average		**11%**

$$\hat{i}_n(k+1) = \left\langle \hat{\mathbf{i}}^{abc}(k+1), \mathbf{s}_2^{abc}(k+1) \right\rangle - \left\langle \hat{\mathbf{i}}^{abc}(k+1), \mathbf{1} \right\rangle, \quad (36)$$

where the current $\hat{\mathbf{i}}^{abc}(k+1)$ can be calculated from (11):

$$\hat{\mathbf{i}}^{abc}(k+1) = \mathbf{T}_{\alpha\beta0-abc}\hat{\mathbf{i}}^{\alpha\beta}(k+1) = \mathbf{T}_{abc-\alpha\beta0}^T\hat{\mathbf{i}}^{\alpha\beta}(k+1). \quad (37)$$

The complete algorithm is summarized in Fig. 5.

C. Comparison between the two controllers

Despite the need of the proposed algorithm to divide the valid states into sub-areas requiring additional calculations, it is computationally simpler and lighter than the conventional FS-MPC. To demonstrate this fact, a comparison is made to illustrate the advantages of the proposal. The total amount of operations in the current or power inner control loop for the FS-MPC and Bee-MPC is presented in Table II, which employs a TMS320F28335 DSP based board to compute the total time as a case study [29], although the procedure can be extended to any other digital board. From Table II, it can be verified that the improvement ratio is about five times for the three-level NPC topology, obtaining equal results.

The proposal operates under the same principle as the conventional one, that is, it finds the state that takes the shortest path to the current or power reference, minimizing at the same time the *dc* voltage difference Δv_{dc}. Neither of them employs any modulation technique such as PWM, and instead the state is directly computed by the controller. As such, the digital board does not require this module and only digital outputs are needed. On the other hand, it has similar disadvantages, as the well-known spread harmonic content typical of the technique. Nevertheless, the quick dynamic response is retained.

The total operations for each algorithm are summarized in TABLE III, detailing the type of operation. As it can be seen, the proposed Bee-MPC uses an average of 11% of the total operations compared to the traditional FS-MPC. Thus, regardless of the digital board used, the computation time is reduced thanks to the improvement in the number of operations. For example, if a slower TMS320F2812, [30], is used, the total time to calculate the FS-MPC will be 107.41 μs and the Bee-MPC 19.05 μs, making it impossible to compute the FS-MPC at $N = 360$ samples per period. In addition, if the Arduino Mega2560 is used, the computing time can go from 14,706 μs to 2,062 μs, which would reduce the samples per period to use the above presented algorithms.

In these algorithms the switching frequency is tied to the sampling frequency, the reduction in computation time allows

the power converter to operate with high switching frequency Silicon Carbide (SiC) technology, increasing the system efficiency, operation at higher temperature, higher breakdown voltage, and many other advantages brought by these new SiC switches.

Nevertheless, it is important to emphasize that the DSP used in this manuscript is an inexpensive one, costing about USD$30. In this comparison, for a grid source operating at 50 Hz, we used $N = 360$ samples per period, corresponding to $T_s = 55.55$ µs for both algorithms. For the 3-level NPC, as shown in Table II, the computation time for the FS-MPC algorithm is 49.34 µs, leaving a short time to execute more instructions such as protection, data acquisition and processing, among others. On the other hand, the proposed Bee-MPC algorithm requires only 8.75 µs, which requires about 20% of the sampling time T_s, which allows increasing the sampling frequency, improving the current and voltage THD, or incorporating new instructions when needed.

D. A conceptual extension to N-level NPC

The application of this technique can be generalized to N-level NPC. To illustrate this in Fig. 6 a 5-level NPC states diagram is shown, highlighting the number of the valid states depending upon the levels and the voltages possibilities. The proposed technique selects the hexagon that includes the voltage vector required to be applied at time $k + 1$, i.e., $\mathbf{v}^{\alpha\beta}(k + 1)$ independent of the inverter levels. The generalized algorithm can be described in the following steps:

i.   *dc*-link voltage control: The *dc*-link voltage is adjusted to operate at MPP, as discussed in Section II.C.

ii.   Power management: The active and reactive power injected by the converter is managed to control the power factor, as described in section II.D.

iii.   MPC to obtain the future voltage value $\mathbf{v}^{\alpha\beta}(k + 1)$: using the power converter model, the predictive control strategy allows to obtain the voltage $\mathbf{v}^{\alpha\beta}$ at $k + 1$ by using equation (19), section II.B.

iv.   Selection of the voltage $\mathbf{v}^{\alpha\beta}(k + 1)$ sector: The hexagon that contains the voltage $\mathbf{v}^{\alpha\beta}(k + 1)$ is found by first selecting the sector (divided into 6 angular regions) by using the equations (22) and (23).

v.   Selection of the voltage $\mathbf{v}^{\alpha\beta}(k + 1)$ hexagon: Once the sector has been defined, the hexagon is found by defining the shapes of the hexagon with lines R^i (slope and vertical lines) in the same way as described in the previous section, equation (24).

vi.   Balancing the *dc*-link capacitor voltages: After finding the hexagon that encloses the desired voltage vector to be applied, the redundant state selection is performed in the direction of balancing the *dc*-link capacitors. This voltage balancing problem is solved by the same optimization techniques of FS-MPC, evaluating all the redundant states.

In general, the Bee-MPC algorithm detects in at most N steps the hexagon surrounding voltage vector, which in the case of FS-MPC method with a N-level NPC must evaluate $1+3N(N−1)$ voltages. Then, for both methods, a subroutine in charge of balancing the *dc* voltage selects the states among the redundances, where in an N-level NPC converter the redundant
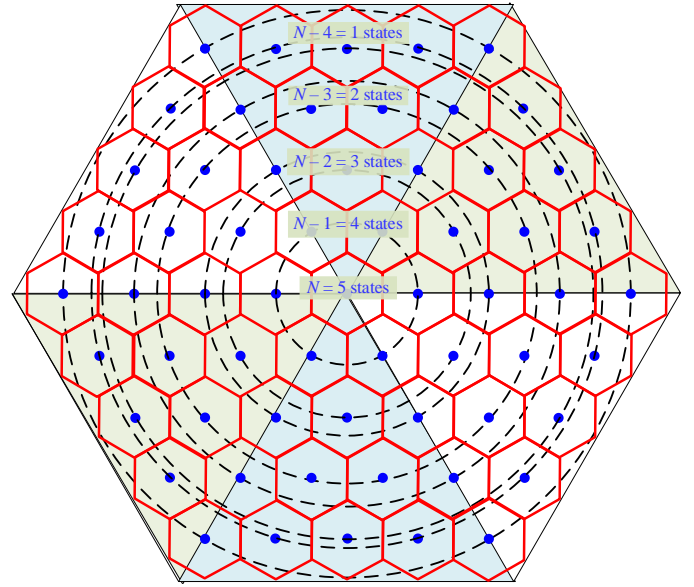

Fig. 6. Valid voltages of an NPC of 5 levels.

states go from N redundant states in the null voltage to the outer states with only one state (see the concentric circles in Fig. 6).

As an example, for $N = 7$ the FS-MPC would evaluate the model 127 times, meanwhile the Bee-MPC only will evaluate 7 lines to reach the desired hexagon after defines $\mathbf{v}^{\alpha\beta}(k + 1)$. In this way, this technique allows a significant reduction in computational effort by directly obtaining the voltage vector to be applied at $k + 1$, independent of the NPC levels, avoiding evaluating all possible voltages as it is done by the FS-MPC. This reduction in computation burden will become much more noticeable as the number of levels of the NPC converter increases, bringing with it the following improvements: better processor utilization, possibility to use higher sampling frequency allowing to reduce the filter size (because the sampling time can be shorter due to the reduction in
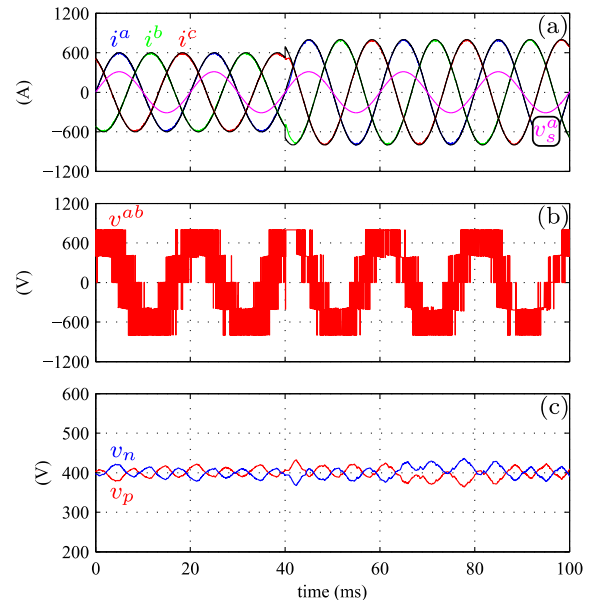

Fig. 7. Step change dynamic response of the controller to a current reference amplitude increase. (a) injected currents $\mathbf{i}^{abc}$ and references, (b) line-to-line voltage v^{ab}, (c) capacitor voltages v_p and v_n.
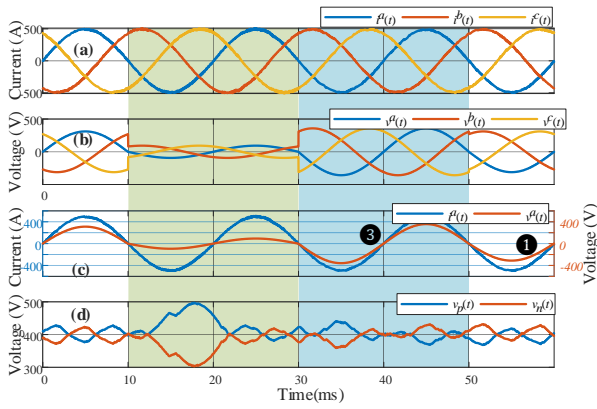
Fig. 8. Grid voltage Sag/swell Bee-MPC response, (a) current i^{abc}, (b) grid voltage, (c) voltage and current v_s^a and $\bar{i}^a$, (d) dc voltage.

computation time), possibility to incorporate new algorithms, such as algorithms for protection of converter power elements.

IV. CONTROLLER TESTS

A. Simulation test

Initially, a simulation test is considered to test the behavior of the proposed controller. A simulation of the system depicted in Fig. 1 is performed using the software PSIM, where the algorithm is implemented as a C language block. The parameters used are $R = 0.5$ mΩ, $L = 1$ mH, $V_s = 220$ Vrms, $C = 4.7$ mF, and $N = 360$ samples per period, leading to $T_s = 55.5$μs for 50 Hz as the grid nominal value. Note that the switching frequency can be as high as the sampling frequency if the states are different in each sampling time, but if the state is repeated one or more times, the switching frequency becomes lower, thus, the switching frequency can go up to 18 kHz.

1) Current control behavior

Step changes in the current reference amplitude are performed, replacing the PV array of Fig. 1 by a constant 800 (V) voltage source. The results are presented in Fig. 7 for an increase in the desired amplitude. From Fig. 7 (a) it can be verified that the references are quickly tracked in approximately 3 ms, as is usually the case with predictive controllers. In addition, the currents are in phase with the grid voltage, operating with unity power factor, as is imposed by the controller. The v^{ab} line-to-line voltage, Fig. 7 (b), has a five-level characteristic as desired in the NPC topology. Besides, the capacitors' voltages are correctly balanced with the proposed strategy, as is illustrated in Fig. 7 (c).

The simulation results obtained under conditions of network disturbances are presented in Fig. 8. To study these types of disturbances, a voltage sag was induced at $t = 10$ms (the grid voltage falls to 30% of the nominal voltage), followed by a voltage swell at $t = 30$ms (the grid voltage rises to 115% of the nominal voltage), and finally, the voltage is restored to the nominal voltage. Throughout the entire duration of the test, the dc voltage and current reference remains constant Fig. 8 (a) and (d). The results demonstrate that the control algorithm successfully maintains both the reference current and the level of capacitor unbalance during nominal voltage (❶), then in the voltage sag (❷) and finally in the voltage swell (❸). Therefore,
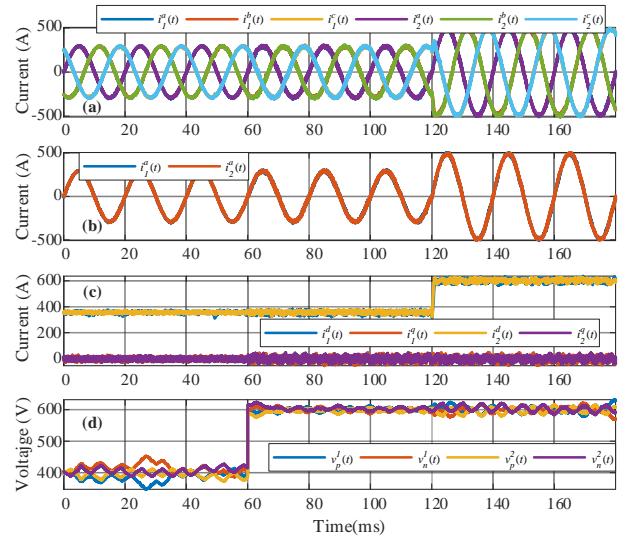

Fig. 9. Comparison between FS-MPC and Bee-MPC, where subscript '1' represents the FS-MPC response and the subscript 2 represents the Bee-MPC response: (a) currents, (b) current of phase a, (c) currents in dq axis, (d) dc link voltages.

it can be concluded that the proposed control algorithm exhibits robustness against grid voltage changes.

To compare the proposed Bee-MPC and the traditional FS-MPC in the time response, Fig. 9 shows the results considering the same inputs with both algorithms. The FS-MPC results are highlighted with the subscript '1' and the Bee-MPC highlighted with the subscript '2'. It is evident that dynamic and static response results are very similar, in fact, can be stated: almost identical, the Bee-MPC THD is 1.68%, while the FS-MPC is 1.75%. Therefore, the proposal does not show significant differences in terms of results, but only in terms of computation time. This is because both algorithms select only one state to be applied in each sampling time, and, therefore, the switching frequency depends on the sampling frequency. Additionally, both algorithms are very fast because they always look for the best state to reach the reference, but the states can be selected two or more times in a row and therefore they do not ensure a concentrate switching spectrum.

B. Experimental Results

To assess the feasibility and correct operation of the proposal tests are made in an experimental setup. The system is composed by an NPC power converter that interfaces a PV array to the grid as shown in Fig. 1 (a). The NPC power converter is implemented by a Microsemi APTGF30TL601G power module, the PV array is implemented by a Magna-Power MagnaDC SL 600-4.3 dc power supply/solar emulator, and the ac mains is provided by a California Instruments 4500iL power source. The control algorithm is implemented in a TMS320F28335 DSP board. The system parameters are $L = 12$ mH, $R = 11$ Ω, $C = 2.2$ mF, $V_s = 15$ V, and $N = 360$ samples per period, leading to $T_s = 55.5$μs for 50 Hz as the grid nominal value; similarly, to the simulation result, the switching frequency can go up to 18 kHz.
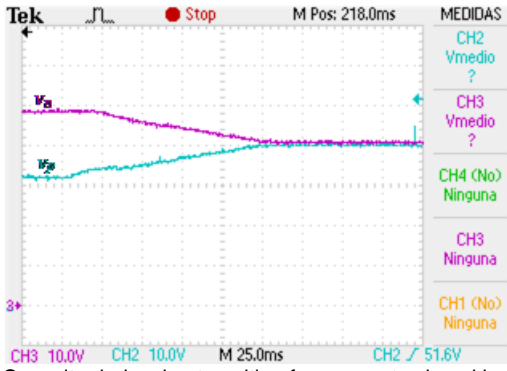
Fig. 10. Capacitor balancing transition from open to closed loop.

1) Capacitor balancing

First, the capacitor balancing operation will be verified using the solar emulator only as a fixed dc power supply. The control algorithm initially operates using only the internal model values of capacitor voltages v_p and v_n, generating the firing signals without considering the true values of the system. Afterwards, at $t = 25$ (ms), the true system variables are measured, and the predictive controller uses the variables in closed loop. The results are presented in Fig. 10. Initially, the voltages are fairly unbalanced, with approximately $v_n = 50$ (V) and $v_p = 30$ (V), and their sum is equal to 80 (V). After the controller uses the true system values, from $t = 25$ (ms), the voltages converge towards approximately the same values, 40 (V), with their sum equals 80 (V) as expected.

2) Reference currents change

After verifying the steady-state operation of the controller, step changes in the reference currents are considered to evaluate its dynamic performance. The total dc voltage is set at 120 (V) for these tests, considering $N = 360$ samples per period, equivalent to a sampling frequency of 18 (kHz). Fig. 11 (a) shows the behavior of the controller when the injected current reference is increased from 1.5 (A) to 2.5 (A). From the results it can be seen that the tracking response of the controller is very fast, where the reference is tracked approximately in 1.5 (ms), which is usually the case when using predictive control.

3) Frequency change

Another test to consider is the operation when the grid frequency changes, which is of particular interest in weak power systems. To assess the controller's behavior under these conditions an increase and decrease in the grid frequency are considered. The dc side voltage is set at 100 V for these tests. The results are presented in Fig. 11 (b). Fig. 11 (b) shows the behavior when the grid frequency is increased from 45 to 55 Hz at instant t_1. From the results it is observed that meanwhile the frequency is changing and the PLL is adapting to the new frequency, the current would have a transitory error, but once the PLL is locked in the new frequency, the current follows its reference rapidly, given that the phase shift between the grid voltage and current is essentially zero.

4) Closed loop operation with PV array and MPPT

Finally, after verifying the correct operation of the scheme with the dc power supply it is possible to test the proposed controller including a PV array. The test considers the injection of power to the grid from a PV array emulated by the solar emulator using the power-voltage characteristics p_{pv}^i, $i = \{1,\ldots,6\}$, shown in Fig. 12 (a). A sequence of changes is programmed in the power supply to be changed every ten seconds and denoted by the numbers $1 - 6$. The operating conditions of the PV array are shown in the power, voltage, and current curves shown in Fig. 12. The results show that the emulated PV array operates under maximum generating conditions at every operating point, denoted by the cross in Fig. 12 (a), as the true output power trajectory (blue) passes over the characteristics. This demonstrates the correct operation of the MPPT, as it generates the voltage reference required to operate at maximum power point, and the entire control system, as the complete system should be controlled to achieve these operating points.

V. CONCLUSIONS

This paper has proposed a new predictive control technique that reproduces the traditional FS-MPC in a three level NPC but reducing the computation time by 80%, as revealed in Table II. The proposal is based on avoiding the iterations of FS-MPC, which tests every valid voltage to choose the one that minimizes a cost function. Instead, the Bee-MPC searches the hexagon where the voltage $\mathbf{v}^{abc}$ is enclosed, directly choosing the state. The proposed technique uses the polar representation of the lines that define every hexagon and with successive searching,
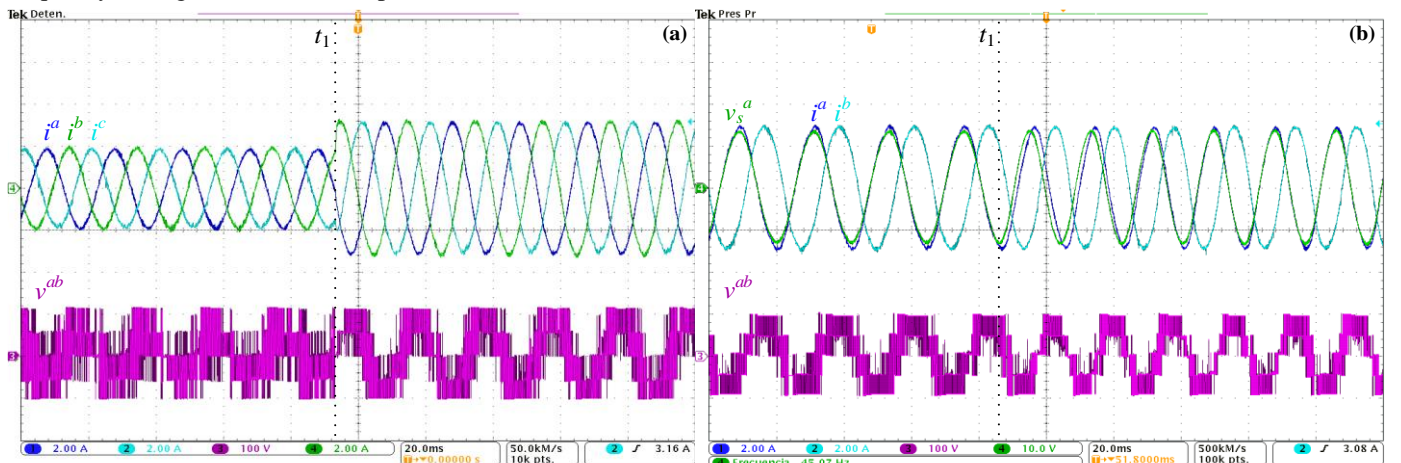

Fig. 11. Controller response to a current reference step change and to a grid frequency disturbance. (a) Current reference increment from 1.5 (A) to 2.5 (A) at time t_1, (b) (a) supply currents i^a, i^b, phase a grid voltage v_s^a, and line-to-line output voltage v^{ab} when the frequency is increased from 45 to 55 Hz.
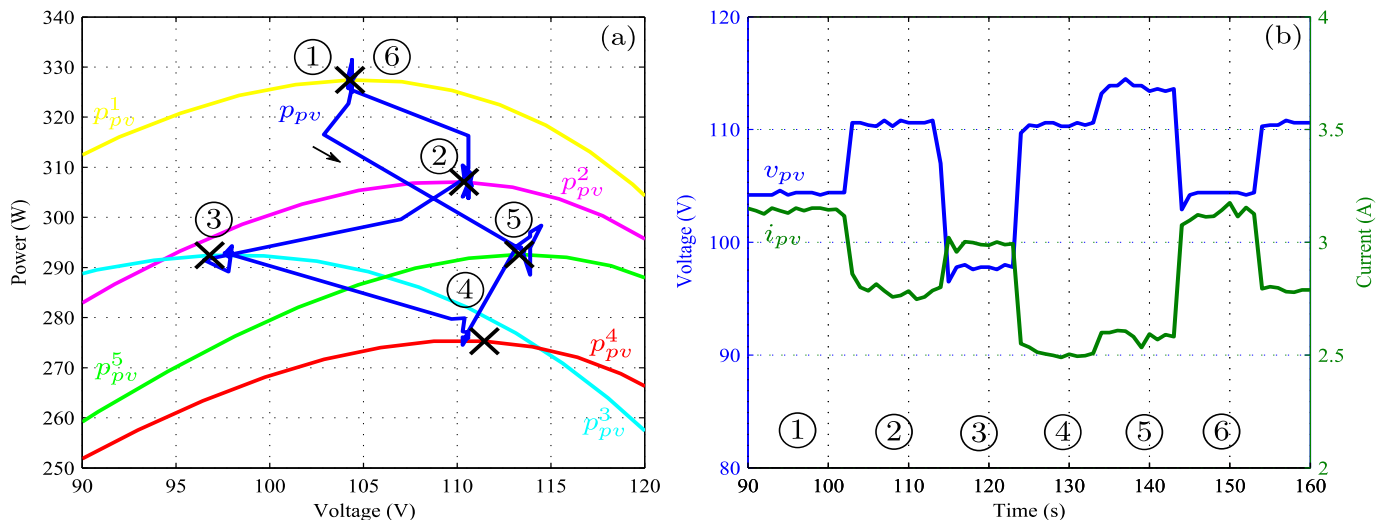
Fig. 12. Operation of the entire PV based system under closed loop with MPPT. (a) power-voltage characteristics and power output of the PV array emulator, (b) voltage and output current of the PV emulator.

the valid NPC voltage is selected. Additionally, it uses the redundant states to regulate the *dc* voltages imbalance. The current THD and the response rapidness are similar to traditional FS-MPC and, therefore, the current performance is not sacrificed to save computing time. The proposal is employed in a grid connected BPV power injection systems. Nonetheless, the applications are related to the three-level NPC capabilities, and therefore can be applied in motor drives, wind power systems, back-to-back topologies, active filters, among many others that use power converters.

VI. REFERENCES

[1] C. D. Rodríguez-Gallegos, M. Bieri, O. Gandhi, J. P. Singh, T. Reindl, and S. K. Panda, "Monofacial vs bifacial Si-based PV modules: Which one is more cost-effective?," *Sol. Energy*, vol. 176, pp. 412–438, Dec. 2018, doi: 10.1016/j.solener.2018.10.012.

[2] A. Kumar, M. Bieri, T. Reindl, and A. G. Aberle, "Economic Viability Analysis of Silicon Solar Cell Manufacturing: Al-BSF versus PERC," *Energy Procedia*, vol. 130, pp. 43–49, Sep. 2017, doi: 10.1016/j.egypro.2017.09.412.

[3] K. Branker, M. J. M. Pathak, and J. M. Pearce, "A review of solar photovoltaic levelized cost of electricity," *Renew. Sustain. Energy Rev.*, vol. 15, no. 9, pp. 4470–4482, Dec. 2011, doi: 10.1016/j.rser.2011.07.104.

[4] J. Johnson, D. Yoon, and Y. Baghzouz, "Modeling and analysis of a bifacial grid-connected photovoltaic system," in *2012 IEEE Power and Energy Society General Meeting*, Jul. 2012, pp. 1–6. doi: 10.1109/PESGM.2012.6345266.

[5] A. Sanchez-Ruiz *et al.*, "DC-Link Neutral Point Control for 3L-NPC Converters Utilizing Selective Harmonic Elimination–PWM," *IEEE Trans. Ind. Electron.*, vol. 69, no. 9, pp. 8633–8644, Sep. 2022, doi: 10.1109/TIE.2021.3113019.

[6] J. Liu *et al.*, "Sliding Mode Control of Grid-Connected Neutral-Point-Clamped Converters Via High-Gain Observer," *IEEE Trans. Ind. Electron.*, vol. 69, no. 4, pp. 4010–4021, Apr. 2022, doi: 10.1109/TIE.2021.3070496.

[7] A. Sanchez-Ruiz *et al.*, "DC-Link Neutral Point Control for 3L-NPC Converters Utilizing Selective Harmonic Elimination–PWM," *IEEE Trans. Ind. Electron.*, vol. 69, no. 9, pp. 8633–8644, Sep. 2022, doi: 10.1109/TIE.2021.3113019.

[8] T. Yu, W. Wan, and S. Duan, "A Modulation Method to Eliminate Leakage Current and Balance Neutral-Point Voltage for Three-Level Inverters in Photovoltaic Systems," *IEEE Trans. Ind. Electron.*, vol. 70, no. 2, pp. 1635–1645, Feb. 2023, doi: 10.1109/TIE.2022.3161809.

[9] F. Donoso, A. Mora, R. Cardenas, A. Angulo, D. Saez, and M. Rivera, "Finite-Set Model-Predictive Control Strategies for a 3L-NPC Inverter Operating With Fixed Switching Frequency," *IEEE Trans. Ind. Electron.*, vol. 65, no. 5, pp. 3954–3965, May 2018, doi: 10.1109/TIE.2017.2760840.

[10] X. Cai, Z. Zhang, J. Zhang, Z. Li, R. Kennel, and Z. Zhang, "Improved Predictive Control of Three-Level-NPC Power Converters," in *2021 IEEE International Conference on Predictive Control of Electrical Drives and Power Electronics (PRECEDE)*, Nov. 2021, pp. 393–402. doi: 10.1109/PRECEDE51386.2021.9680960.

[11] A. Ja'afari *et al.*, "Voltage Balancing of NPC Converter Capacitors in FS-MPC Method Using Current Sensor with Reduction of Computational Burden," in *2021 IEEE International Conference on Predictive Control of Electrical Drives and Power Electronics (PRECEDE)*, Nov. 2021, pp. 218–223. doi: 10.1109/PRECEDE51386.2021.9680939.

[12] N. Jin, D. Dai, H. Xie, J. Wu, and L. Guo, "Virtual Vector-Based FCS-MPC for NPC Three-Level Grid-Tied Inverter Without Weighting Factor of Neutral-Point Voltage Balancing," *IEEE Access*, vol. 10, pp. 72806–72814, 2022, doi: 10.1109/ACCESS.2022.3187994.

[13] J. J. Silva, J. R. Espinoza, J. A. Rohten, E. S. Pulido, F. A. Villarroel, and M. L. Andreu, "A Novel Simplified Implementation of Finite-Set Model Predictive Control for Power Converters," *IEEE Access*, vol. 9, pp. 96114–96124, 2021, doi: 10.1109/ACCESS.2021.3094864.

[14] Z. Zhao *et al.*, "Hierarchical Pigeon-Inspired Optimization-Based MPPT Method for Photovoltaic Systems Under Complex Partial Shading Conditions," *IEEE Trans. Ind. Electron.*, vol. 69, no. 10, pp. 10129–10143, Oct. 2022, doi: 10.1109/TIE.2021.3137595.

[15] M. H. Mobarak and J. Bauman, "A Fast Parabolic-Assumption Algorithm for Global MPPT of Photovoltaic Systems Under Partial Shading Conditions," *IEEE Trans. Ind. Electron.*, vol. 69, no. 8, pp. 8066–8079, Aug. 2022, doi: 10.1109/TIE.2021.3109515.

[16] R. H. Morales *et al.*, "A Novel Global Maximum Power Point Tracking Method Based on Measurement Cells," *IEEE Access*, vol. 10, pp. 97481–97494, 2022, doi: 10.1109/ACCESS.2022.3205163.

[17] J. Silva, J. Espinoza, J. Rohten, M. Torres, and E. Espinosa, "Grid connected PV system with maximum power point estimation based on reference cells," *IECON 2015 - 41st Annu. Conf. IEEE Ind. Electron. Soc.*, no. 2, pp. 4070–4075, 2015, doi: 10.1109/IECON.2015.7392734.

[18] A. Ja'afari *et al.*, "Voltage Balancing of NPC Converter Capacitors in FS-MPC Method Using Current Sensor with Reduction of Computational Burden," in *2021 IEEE International Conference on Predictive Control of Electrical Drives and Power Electronics (PRECEDE)*, Nov. 2021, pp. 218–223. doi: 10.1109/PRECEDE51386.2021.9680939.

[19] X. Cai, Z. Zhang, J. Zhang, Z. Li, R. Kennel, and Z. Zhang, "Improved Predictive Control of Three-Level-NPC Power Converters," in *2021 IEEE International Conference on Predictive Control of Electrical Drives and Power Electronics (PRECEDE)*, Nov. 2021, pp. 393–402. doi:

10.1109/PRECEDE51386.2021.9680960.

[20] J. A. Rohten *et al.*, "A Simple Self-Tuning Resonant Control Approach for Power Converters Connected to Micro-Grids With Distorted Voltage Conditions," *IEEE Access*, vol. 8, pp. 216018–216028, 2020, doi: 10.1109/ACCESS.2020.3041528.

[21] P. Karamanakos and T. Geyer, "Guidelines for the Design of Finite Control Set Model Predictive Controllers," *IEEE Trans. Power Electron.*, vol. 35, no. 7, pp. 7434–7450, Jul. 2020, doi: 10.1109/TPEL.2019.2954357.

[22] P. Karamanakos, E. Liegmann, T. Geyer, and R. Kennel, "Model Predictive Control of Power Electronic Systems: Methods, Results, and Challenges," *IEEE Open J. Ind. Appl.*, vol. 1, pp. 95–114, 2020, doi: 10.1109/OJIA.2020.3020184.

[23] P. Karamanakos, E. Liegmann, T. Geyer, and R. Kennel, "Model Predictive Control of Power Electronic Systems: Methods, Results, and Challenges," *IEEE Open J. Ind. Appl.*, vol. 1, pp. 95–114, 2020, doi: 10.1109/OJIA.2020.3020184.

[24] P. Cortes, J. Rodriguez, C. Silva, and A. Flores, "Delay Compensation in Model Predictive Current Control of a Three-Phase Inverter," *IEEE Trans. Ind. Electron.*, vol. 59, no. 2, pp. 1323–1325, Feb. 2012, doi: 10.1109/TIE.2011.2157284.

[25] M.-V. Doi, B.-X. Nguyen, and N.-V. Nguyen, "A Finite Set Model Predictive Current Control for Three-Level NPC Inverter with Reducing Switching State Combination," in *2019 IEEE 4th International Future Energy Electronics Conference (IFEEC)*, Nov. 2019, pp. 1–9. doi: 10.1109/IFEEC47410.2019.9015021.

[26] X. Zhang, G. Tan, T. Xia, Q. Wang, and X. Wu, "Optimized Switching Finite Control Set Model Predictive Control of NPC Single-Phase Three-Level Rectifiers," *IEEE Trans. Power Electron.*, vol. 35, no. 10, pp. 10097–10108, Oct. 2020, doi: 10.1109/TPEL.2020.2978185.

[27] Z. Liu, Z. Xia, D. Li, Y. Wang, and F. Li, "An Optimal Model Predictive Control Method for Five-Level Active NPC Inverter," *IEEE Access*, vol. 8, pp. 221414–221423, 2020, doi: 10.1109/ACCESS.2020.3043604.

[28] C. Xue, D. Zhou, and Y. Li, "Finite-Control-Set Model Predictive Control for Three-Level NPC Inverter-Fed PMSM Drives With LC Filter," *IEEE Trans. Ind. Electron.*, vol. 68, no. 12, pp. 11980–11991, Dec. 2021, doi: 10.1109/TIE.2020.3042156.

[29] M. P. Kazmierkowski, M. Jasinski, and G. Wrona, "DSP-Based Control of Grid-Connected Power Converters Operating Under Grid Distortions," *IEEE Trans. Ind. Informatics*, vol. 7, no. 2, pp. 204–211, May 2011, doi: 10.1109/TII.2011.2134856.

[30] M. Pasko, M. Maciazek, and D. Bula, "Performance and accuracy comparison of fixed and floating-point realizations of the Active Power Filter control algorithm," in *2008 International School on Nonsinusoidal Currents and Compensation*, Jun. 2008, pp. 1–4. doi: 10.1109/ISNCC.2008.4627502.